Two-neutron transfer reaction mechanisms in ^{12}C(^{6}He,^{4}He)^{14}C using a realistic three-body ^{6}He model

D. Smalley,[1,*] F. Sarazin,[1] F. M. Nunes,[2,3] B. A. Brown,[2,3] P. Adsley,[4] H. Al-Falou,[5] C. Andreoiu,[6] B. Baartman,[6] G. C. Ball,[5] J. C. Blackmon,[7] H. C. Boston,[8] W. N. Catford,[9] S. Chagnon-Lessard,[10] A. Chester,[6] R. M. Churchman,[5] D. S. Cross,[6] C. Aa. Diget,[4] D. Di Valentino,[11] S. P. Fox,[4] B. R. Fulton,[4] A. Garnsworthy,[5] G. Hackman,[5] U. Hager,[1] R. Kshetri,[6] J. N. Orce,[5] N. A. Orr,[12] E. Paul,[8] M. Pearson,[5] E. T. Rand,[10] J. Rees,[8] S. Sjue,[5] C. E. Svensson,[10] E. Tardiff,[5] A. Diaz Varela,[10] S. J. Williams,[2] and S. Yates[13]

[1]*Department of Physics, Colorado School of Mines, Golden, Colorado 80401, USA*
[2]*National Superconducting Cyclotron Laboratory, Michigan State University, East Lansing, Michigan 48824, USA*
[3]*Department of Physics and Astronomy, Michigan State University, East Lansing, Michigan 48824, USA*
[4]*Department of Physics, University of York, York YO10 5DD, United Kingdom*
[5]*TRIUMF, Vancouver V6T 2A3, British Columbia, Canada*
[6]*Department of Chemistry, Simon Fraser University, Burnaby V5A1S6, British Columbia, Canada*
[7]*Department of Physics and Astronomy, Louisiana State University, Baton Rouge, Louisiana 70803, USA*
[8]*Department of Physics, University of Liverpool, Liverpool L69 3BX, United Kingdom*
[9]*Department of Physics, University of Surrey, Guildford GU15XH, United Kingdom*
[10]*Department of Physics, University of Guelph, Guelph N1G 2W1, Ontario, Canada*
[11]*Department of Physics, Carleton University, Ottawa K1S 5B6, Ontario, Canada*
[12]*LPC-ENSICAEN, IN2P3-CNRS et Université de Caen, 14050 Caen Cedex, France*
[13]*Department of Physics, University of Kentucky, Lexington, Kentucky 40506, USA*

The reaction mechanisms of the two-neutron transfer reaction ^{12}C(^{6}He,^{4}He) have been studied at $E_{lab} =$ 30 MeV at the TRIUMF ISAC-II facility using the Silicon Highly-segmented Array for Reactions and Coulex (SHARC) charged-particle detector array. Optical potential parameters have been extracted from the analysis of the elastic scattering angular distribution. The new potential has been applied to the study of the transfer angular distribution to the 2_2^+ 8.32 MeV state in ^{14}C, using a realistic three-body ^{6}He model and advanced shell-model calculations for the carbon structure, allowing to calculate the relative contributions of the simultaneous and sequential two-neutron transfer. The reaction model provides a good description of the 30-MeV data set and shows that the simultaneous process is the dominant transfer mechanism. Sensitivity tests of optical potential parameters show that the final results can be considerably affected by the choice of optical potentials. A reanalysis of data measured previously at $E_{lab} =$ 18 MeV, however, is not as well described by the same reaction model, suggesting that one needs to include higher-order effects in the reaction mechanism.

I. INTRODUCTION

One of the critical ingredients to understanding nuclear properties, both in the valley of stability and at the nuclear drip lines, is the pairing effect [1]. Pairing is a general term that embodies the correlation between pairs of nucleons, producing, for example, the well-known mass staggering in nuclear isobars. Pairing is also essential to understanding the formation of two-neutron halos [2]. Although the importance of pairing for describing nuclear phenomena is well accepted, the reaction probes used to measure pairing are still poorly understood.

Two-nucleon transfer is the traditional probe used to study pairing. The main idea is that the angular distribution for the simultaneous transfer of two nucleons depends directly on the change in the angular momentum of the two nucleons from the original to the final nucleus, and therefore provides indirectly information on their relative motion. Experimental studies of two-neutron transfer imply the use of a surrogate reaction. Hence, the interpretation of the results become strongly dependent on the reaction mechanism since typically the simultaneous transfer of the two nucleons is contaminated by the two-step sequential transfer.

Traditionally $A(t,p)B$ or $B(p,t)A$ reactions have been the most common tools used to explore two-neutron correlations (see, for example, Refs. [3,4] for earlier studies and Refs. [5,6] for more recent studies). The advantage of (t,p) is that it allows the study of not only the ground state of B but also of a number of its excited states, accessible through energy and angular momentum matching. Since the triton is a well understood nucleus, it was thought that these reactions would be easier to describe than others using heavier probes [7,8]. However, missing factors of 2 or 3 in the cross section normalization (known as the unhappiness factor [9,10]) for (p,t) and (t,p) have shown that a simple perturbative description that does not take into account the intermediate deuteron state correctly

---

*Present address: The National Superconducting Cyclotron Laboratory, Michigan State University, East Lansing, MI 48824, US; smalleyd@nscl.msu.edu

has severe limitations [1]. There are experimental drawbacks as well: (p,t) only permits the study of the ground state of the original nucleus considered and (t,p) requires the handling of tritium radioactivity, which is challenging in most laboratories.

Other two-neutron transfer probes have been considered. The next simplest case after (t,p) would be the $(^6\text{He},^4\text{He})$ reaction involving the two-neutron halo nucleus ^6He. The structure of ^6He makes it a very attractive candidate for two-neutron transfer reactions because of its Borromean nature and its very low two-neutron separation energy ($S_{2n} = 0.97$ MeV). Indeed, Chatterjee *et al.* [11] recently observed in ^6He on ^{65}Cu at 23 MeV a large dominance of the two-neutron over one-neutron transfer cross section and interpreted this in terms of the unique features of the ^6He wave function. At present, ^6He is the best understood two-neutron halo nucleus, with a very significant component where the halo neutrons are spatially correlated (the so-called "dineutron" component) and an equally important component where the two halo neutrons are anticorrelated (the so-called "cigar" component) (see, e.g., Refs. [12,13]). Given the comparatively small ^6He two-neutron separation energy with respect to the one of the triton ($S_{2n} = 6.25$ MeV), the two-neutron transfer reaction $(^6\text{He},^4\text{He})$ provides not only a higher Q value overall than its (t,p) counterpart allowing for higher excited states to be populated, but also a more favorable Q-value matching condition for a given two-neutron transfer reaction. It has even been suggested by Fortunato *et al.* [14] that this higher Q value provides relatively large cross sections to study giant pairing vibrations in heavy ions. It also provides a different angular momentum matching condition, given that the two active neutrons can exist in a relative p state as opposed to the situation in the triton. In addition to these two important differences, the Borromean nature of ^6He [15] implies that the sequential transfer can only happen through the continuum states of ^5He and is likely to leave a softer imprint in the distributions than the sequential process in (t,p) through the deuteron bound state.

Experimentally, the major drawback lies in the fact that ^6He is unstable ($T_{1/2} = 807$ ms) and therefore the reaction can only be studied using targets made of stable or long-lived isotopes. Theoretically, one difficulty arises from the existence of unbound excited states in ^6He, the first one (2^+) at 1.8 MeV. With this in mind, what is needed to explore $(^6\text{He},^4\text{He})$ is a test case, where the final state is well understood, such that the focus can be on the reaction mechanism.

Given the interest in the halo structure of ^6He [15,16], there have been many measurements involving the $(^6\text{He},^4\text{He})$ vertex. The measurements of the $p(^6\text{He},^4\text{He})t$ at 151 MeV [17,18] resulted in difficulties in the analysis due to the strong interference of the small $t + t$ component in the ^6He wave function. There were also two measurements on $^4\text{He}(^6\text{He},^4\text{He})^6\text{He}$, one at $E_\text{lab} = 29$ MeV [19] and the other at $E_\text{lab} = 151$ MeV [20]. In this reaction, the transfer channel corresponds to the exchange of the elastic channel, reducing the number of effective interactions necessary to describe the process, but introducing yet another complication, that of appropriate symmetrization. And while the authors of Ref. [11] clearly demonstrated a preference for two-neutron over

one-neutron transfer, the actual mechanism for the two-neutron transfer was simply assumed to be one-step arising from the dineutron configuration of the ^6He wave function.

Our test case is the reaction $^{12}\text{C}(^6\text{He},^4\text{He})^{14}\text{C}$, a reaction that populates well-known states in ^{14}C. Possible intermediate states in ^{13}C in the sequential transfer are also well known. If we thus assume that our present knowledge of ^6He is complete, we can focus on the reaction mechanism. $^{12}\text{C}(^6\text{He},^4\text{He})^{14}\text{C}$ was first performed at $E = 5.9$ MeV [21] and populated the ground state and the first 1^- and 3^- states in ^{14}C. Following that measurement, the reaction was remeasured at 18 MeV [22], populating strongly the 8.32 MeV 2^+_2 state in ^{14}C. At the lowest beam energy, the transfer cannot be treated perturbatively, resulting in an intricate mechanism for the process [23], in Ref. [22] a reasonable description of the reaction was provided with the simple one-step dineutron model.

In this work, we present new results from the measurement of $^{12}\text{C}(^6\text{He},^4\text{He})^{14}\text{C}$ at 30 MeV and discuss in detail the reaction mechanisms, taking into account not only the one-step but also two-step (through intermediate ^{13}C states) processes. The new model is also applied to the previous study at 18 MeV. In Sec. II, we describe the experimental setup and details in the analysis. In Sec. III, we briefly summarize the main ingredients used in the reaction theory used to analyze our results. The elastic scattering results are presented in Sec. IV A, followed by the inelastic scattering in Sec. IV B and the transfer results in Sec. IV C. Finally, in Sec. V we summarize and draw our conclusions.

II. EXPERIMENTAL SETUP

The $^{12}\text{C}(^6\text{He},^4\text{He})^{14}\text{C}$ experiment was performed in direct kinematics at the TRIUMF ISAC-II facility using a combination of the Silicon Highly-segmented Array for Reactions and Coulex (SHARC) [24] and the TRIUMF-ISAC Gamma-Ray Escape-Suppressed Spectrometer (TI-GRESS) [25]. The $^6\text{He}^+$ beam was produced by impinging a 500-MeV, 75-μA proton beam upon a 20.63 g/cm^2 ZrC target, and extracted using a forced electron beam induced arc discharge (FEBIAD) ion source. The 12.24 keV ^6He beam was postaccelerated through the ISAC-I (where the beam was also stripped to 2+) and ISAC-II accelerators to 30 MeV before being delivered to the TIGRESS beam line. A small amount ($<5\%$) of ^6Li contaminant was also transmitted through the accelerator. The beam then impinged upon a 217 μg/cm^2 ^{12}C target located at the center of the SHARC and TIGRESS arrays. The average beam intensity was estimated to be $I = 8 \times 10^5$ pps with a total integrated beam current on target of 77 nC over the course of the experiment.

The laboratory angular coverage of the SHARC array is shown in Fig. 1, where each point represents a pixel of detection. The downstream end cap detectors (DCD) consisted of four ΔE-E telescopes made of three 80-μm double-sided silicon strip detectors (DSSSD) and one single-sided 40-μm ΔE detector, all backed with 1-mm E detectors. The polar angle coverage in the laboratory frame of the DCD was
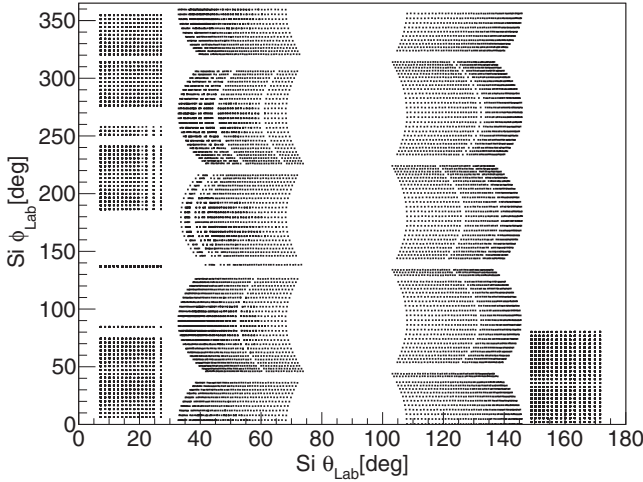
FIG. 1. Laboratory angular coverage of SHARC for this experiment. The areas of detection are the downstream end cap (DCD) at $7° < \theta_{lab} < 27°$, the downstream box (DBx) at $32° < \theta_{lab} < 71°$, the upstream box (UBx) at $103° < \theta_{lab} < 145°$, and the partial upstream end cap (UCD) at $148° < \theta_{lab} < 172°$. One of the DCD detectors was single-sided, hence the single row of pixels along the θ_{lab} direction at $135° < \phi_{lab} < 140°$, which depicts the center ϕ_{lab} angle used for reconstruction (the coverage was $100° < \phi_{lab} < 175°$).

$7°$–$27°$. The downstream box (DBx) was comprised of four 140-μm DSSSDs ΔE detectors backed with 1.5-mm E detectors and polar angle coverage of $32°$–$71°$. The upstream box (UBx) was made of four 1-mm DSSSDs with polar angle coverage of $103°$–$145°$. Finally, the partial upstream end cap (UCD) consisted of a single 1-mm DSSSD with a polar angle coverage of $148°$–$172°$. A total of 21 strips out of 752 were not functioning, giving a solid angle coverage of the array of $\Omega \approx 2\pi$. Additionally, one DCD E ($184° < \phi_{lab} < 258°$) detector malfunctioned during the experiment.

Particle identification was obtained for three quadrants of DCD and all quadrants of DBx. The DCD ΔE-E provided identification of all the isotopes of charge $Z \leqslant 3$ as shown in Fig. 2. In particular, clear separation of the ^{4}He and ^{6}He isotopes was achieved allowing for a clear identification of the elastic/inelastic scattering from the two-neutron transfer (and fusion-evaporation) channels. Only the identification of particles with mass $A \leqslant 4$ was possible in the downstream box due to the thickness of the ΔE detectors (which stopped the scattered ^{6}He beam). For UBx and UCD, identification of the two-neutron transfer channel remained possible because of the high Q value of the reaction ($Q = 12.15$ MeV).

The TIGRESS array was used in high-efficiency mode for γ-ray detection. The angular coverage of the TIGRESS array was such that there were seven clover detectors at $\theta_{lab} = 90°$ and four clover detectors at $\theta_{lab} = 135°$ with one crystal not operational in the clover at ($\theta_{lab} = 135°$, $\phi_{lab} = 113°$). The detection of γ rays in coincidence with charged particles was achieved, but the statistics was too low to carry out analyses of γ-gated angular distributions. In what follows, γ-ray detection and tagging are not discussed further.
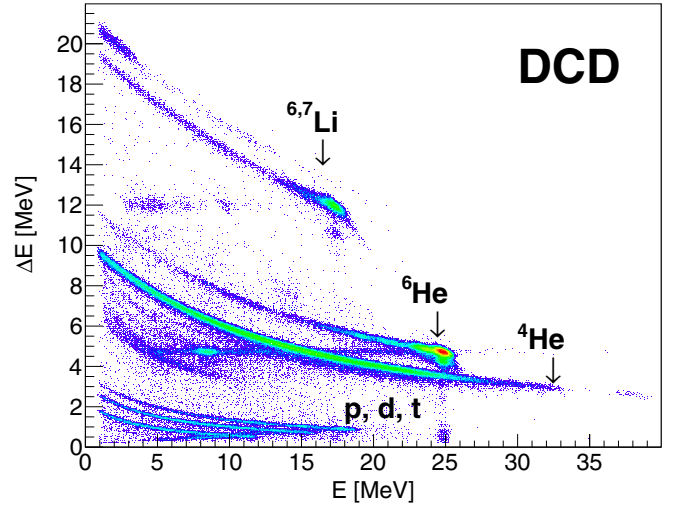

FIG. 2. (Color online) Particle identification for the DCD. The ΔE-E plot shows the energy loss in the thin 80-μm detector (ΔE) plotted against the energy loss in the thick 1-mm detector (E). The nuclei unambiguously identified are shown in the figure.

III. THEORY

A. Reaction mechanisms

We study two-neutron transfer with the finite-range distorted wave Born approximation (DWBA). The simultaneous two-neutron transfer process is treated to first order, as one step (see, e.g., Ref. [26] for details). The transition amplitude for the process for ^{12}C(^{6}He,^{4}He)^{14}C(2^+) can be written as [26]

$$T^{post} = \langle \chi_f \, \mathcal{I}_{^{14}C,^{12}C} | \Delta V | \mathcal{I}_{^6He,^4He} \, \chi_i \rangle, \qquad (1)$$

where χ_i and χ_f are the initial and final distorted waves between ^{6}He-^{12}C and ^{4}He-^{14}C, respectively, and $\mathcal{I}_{He}$ and $\mathcal{I}_C$ are the two-neutron overlap functions of the ground state of ^{6}He and ^{4}He, and the 2_2^+ state of ^{14}C and the ground state of ^{12}C, respectively. In the post form [27], the potential is defined as

$$\Delta V = V_{2n^{12}C} + V_{\alpha^{12}C} - U_i, \qquad (2)$$

where $V_{2n^{12}C}$ is the potential between the two valence neutrons of the ^{6}He and the ^{12}C, $V_{\alpha^{12}C}$ is the core-core potential and U_i is the entrance channel potential (^{6}He + ^{12}C).

Many analyses of two-neutron transfer data involving ^{6}He beams have assumed that the ^{6}He system can be described by a two-body wave function of the α particle and a dineutron cluster, simplifying tremendously the two-neutron overlap function needed in the transfer matrix element (see, e.g., Refs. [11,22]). While a full six-body microscopic description [13,28] may not provide more than a correction to the overall normalization of the overlap function, the three-body ^{6}He $= {}^4$He $+ n + n$ wave function is a requirement for a consistent treatment of simultaneous and sequential transfer, present for all but the highest energies $E > 100$ MeV. In this work, we use a realistic three-body model for ^{6}He [29], which reproduces the binding energy and radius of the ground state. The two-neutron spectroscopic amplitudes for ^{14}C are obtained from microscopic shell-model calculations, which we describe

in more detail below. We assume a standard geometry (radius $r = 1.25$ fm and diffuseness $a = 0.65$ fm) for the mean field generating the radial form factor including a spin-orbit with the same geometry as the mean field and a strength of $V = 6.5$ MeV for the ^{14}C two-neutron overlap function.

The initial and final distorted waves are also important elements of Eq. (1). One way to constrain these is by using elastic scattering over a wide angular range. For the optical potential in the final channel ^{4}He-^{14}C, there are many possible data sets from which to draw, and even global parametrizations may be adequate since none of the nuclei involved are of a peculiar structure. The same is not true for the initial channel. Separate studies on the elastic scattering of ^{6}He on ^{12}C [30,31] at high energies have revealed very significant modifications of the expected optical potential based on the double folding approach due to the large breakup effects inherent to the low S_{2n} of ^{6}He. Given the strong dependence of the two-neutron transfer cross section on the optical potentials used, it is critical to have elastic scattering data at the appropriate energy for a meaningful analysis. This is presented in Sec. IV A.

At the energies we are interested in, the two-step sequential process must be considered. In this case we need to include the one-nucleon transfer into ^{13}C as follows:

$$T^{\text{post}} = \langle \chi_{f1} \, \mathcal{I}_{^{13}\text{C},^{12}\text{C}} | \Delta V_1 | \mathcal{I}_{^6\text{He},^5\text{He}} \, \chi_{i1} \rangle, \tag{3}$$

where the initial state of Eq. (1) is taken into a bound state in ^{13}C and followed by the second neutron transferring from ^{5}He to the final state in ^{14}C as follows:

$$T^{\text{prior}} = \langle \chi_{f2} \, \mathcal{I}_{^{14}\text{C},^{13}\text{C}} | \Delta V_2 | \mathcal{I}_{^5\text{He},^4\text{He}} \, \chi_{i2} \rangle. \tag{4}$$

A number of ^{13}C states contribute to this process, and the needed spectroscopic amplitudes are obtained from microscopic shell-model calculations, assuming the same residual interaction and model space as that used for the two-neutron amplitudes. We avoid the explicit inclusion of states in the continuum by modifying the binding energy and level scheme of ^{13}C.

B. Shell-model considerations for carbon overlaps

All structural information for the carbon isotopes relies on recent shell-model predictions. The earliest discussion related to the structure of the 2^+ 8.32 MeV state in ^{14}C is based on the gamma decay of its analog in ^{14}N at 10.43 MeV [32]. There are two 2^+ $T = 1$ states in this energy region of ^{14}N, the 10.43 MeV and a lower one at 9.16 MeV. The possible shell-model configurations for these states relative to a closed shell for ^{16}O are two holes in the p shell ($2h$) and four holes in the p shell with two particles in the sd shell ($2p$-$4h$). The electromagnetic decay required about an equal admixture between these two configurations. The early weak-coupling model of Lie [33] could reproduce this result only by introducing an empirical energy shift in the $2p - 4h$ component. Mordechai *et al.* [34] used the empirical wave functions of Lie to understand the relative ^{12}C$(t,p)^{14}$C strength to the 7.01 and 8.32 MeV 2^+ states. The (t,p) cross section is dominated by the $2p$ (sd) part of the transfer, and the mixing results in about equal (t,p) cross sections for these two 2^+ states.

Here we are able to use the full p–sd model space. In this model space the basis dimension is 982 390 for $J = 2$, and the wave functions can be obtained with the NuShellX code [35]. A Hamiltonian for this space was recently developed by Utsuno and Chiba [36] (psdUC). This was used to calculate Gamow-Teller strengths for the ^{12}B$(^7$Li,^{7}Be$)^{12}$Be reaction. Relative to the original Hamiltonian of Utsuno and Chiba, the p–sd gap had to be increased by 1 MeV to reproduce the correct mixing of states in ^{12}Be. We calculated the two-particle transfer amplitudes with this same modified psdUC Hamiltonian. The wave functions for the two 2^+ states in ^{14}C came out with about the correct mixing between $2h$ and $2p - 4h$ that are required to reproduce the gamma decay and the relative (t,p) cross sections. The theoretical energy splitting of 0.51 MeV is smaller than the experimental value of 1.3 MeV. But the most important aspect for the present analysis is that the structure of the 2^+ state be consistent with the history of its structure that we have outlined above.

C. Details of the calculations

The level scheme relevant for the transfer is shown in Fig. 3(a) with the Q values listed. A direct transfer from the ground state of ^{6}He to the 2_2^+ 8.32 MeV state in ^{14}C is shown with a solid line. The sequential transfer paths, represented by dashed lines, involve single particle overlaps. To reduce the complexity of the reaction theory and associated
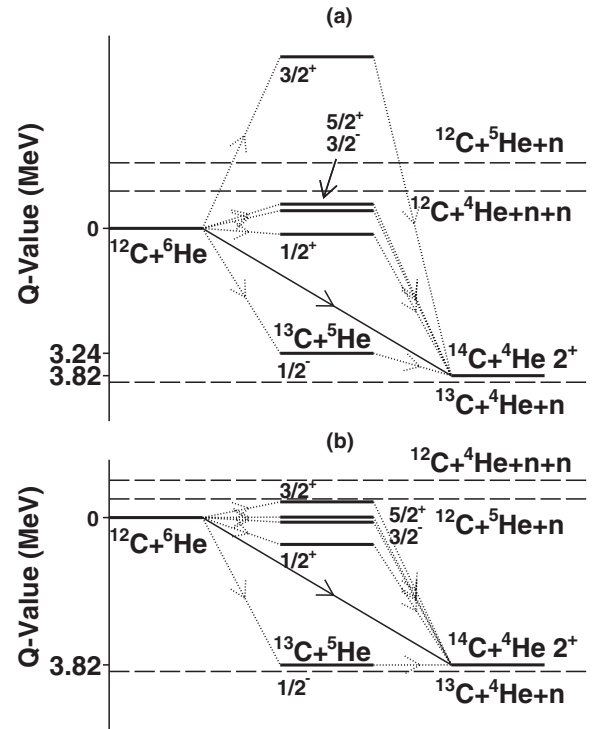

FIG. 3. The level scheme adopted for this two-neutron transfer study. The solid line shows the pathway for simultaneous transfer. The dotted lines show the multiple pathways taken into account in the sequential transfer. The total transfer calculation then takes the coherent sum of all the pathways. The true level scheme is shown in (a) and the modified level scheme which was used is depicted in (b).

computational cost, we make a quasibound approximation for ^{5}He, and take for the ^{5}He optical potentials, the same parameters used for ^{6}He-^{12}C. The binding energy of the quasibound ^{5}He was assumed to be half the binding energy of ^{6}He relative to ^{4}He (28.7831 MeV). Similarly, we slightly shifted the intermediate ^{13}C states to avoid introducing the continuum in our calculations. The only significant shift introduced was for the high lying $3/2^+$ state. Although the relative spectroscopic amplitudes for the ^{13}C $3/2^+$ state is weak compared to the most dominant states of $5/2^+$ and $1/2^+$, we found that this state has a nonnegligible contribution to the cross section. The total transfer calculation is then the coherent sum of all the pathways. Figure 3(b) shows the final level scheme adopted in our reaction calculation. The indirect route of the unbound 2^+ excited state of ^{6}He was not considered. Krouglov *et al.* [23] observed that in the analysis of the ^{6}He + ^{12}C two-neutron transfer at $E_{\mathrm{lab}} = 5.9$ MeV it was of minor importance.

The transfer calculations were performed using the reaction code FRESCO [37] and the realistic three-body calculations for ^{6}He were performed using EFADD [38]. The integration was performed out to 30 fm and the transfer matrix element nonlocality was calculated out to 10 fm. The cluster variable for the two-neutron overlap extended to 10 fm and partial waves up to $J_{\mathrm{max}} = 33$ were included, for convergence.

IV. RESULTS AND DISCUSSION

A. Elastic scattering

The elastic scattering angular distribution was extracted for the downstream ($\theta_{\mathrm{lab}} < 90°$) detection system. For $\theta_{\mathrm{lab}} > 90°$, no clear identification of the elastic scattering channel could be achieved. Figure 4 shows the energy versus θ_{lab} in the DCD and DBx for the ^{6}He + ^{12}C elastic and inelastic scatterings after cuts on the data. In the DCD, unambiguous identification of the scattered ^{6}He was achieved through ΔE-E particle identification. The elastic angular distribution was only extracted past $\theta_{\mathrm{lab}} = 10.7°$ because of the presence of elastic scattering on a heavy nucleus in the first three polar strips. As mentioned earlier, (in)elastically scattered ^{6}He does not punch-through the ΔE in the DBx. However, clean identification of the scattering events could still be achieved using kinematics considerations. For this particular reaction, both the scattered ^{6}He and recoiling ^{12}C remain confined to the DBx and are detected in a reaction plane intersecting opposite DBx quadrants. Using cuts on the kinematic correlation of the ^{6}He and ^{12}C energies, polar angles θ and azimuthal angles ϕ, the kinematic loci for ^{6}He and ^{12}C were extracted from the background and are shown in Fig. 4. The detection of ^{12}C in the DBx stops abruptly at $\theta_{\mathrm{lab}} = 36°$ due to the ^{6}He scattering beyond $\theta_{\mathrm{lab}} = 72°$. Monte Carlo simulations using GEANT4 [42] were performed to determine the detection efficiency arising from these cuts and to normalize the DCD and DBx relative angular distributions.

The elastic scattering angular distribution is shown in Fig. 5 (top). The absolute cross section was obtained by normalizing the angular distribution to Coulomb scattering at forward angles. Only statistical errors are shown, but we estimate
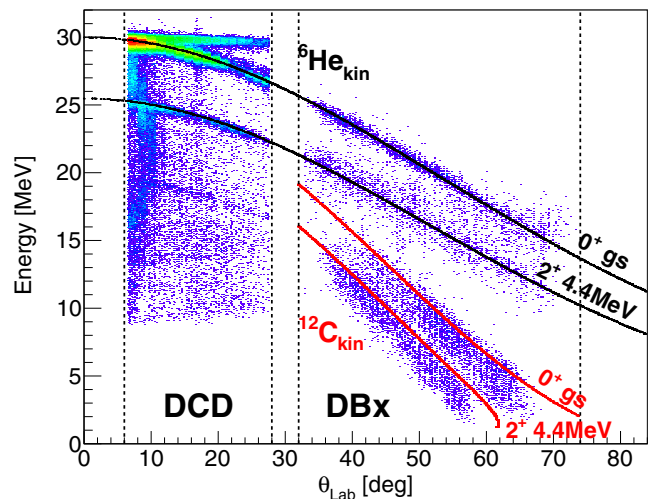

FIG. 4. (Color online) The elastic and inelastic scattering energy vs. θ_{lab} kinematics. The DCD used the straightforward particle ID of the ^{6}He ejectiles, while the DBx required coincident detection considerations (see text for details). The kinematic curves for ^{6}He and ^{12}C are shown in black and red, respectively, with strong population of the 0^+ ground state and the 2^+ 4.4 MeV state of ^{12}C. The slight mismatch in energy of the ^{12}C expected kinematics is due to increased energy loss from the higher Z and straggling in the carbon target.

a systematic error in the normalization of 25%. The solid line is the optical model obtained from a χ^2 minimization of the ^{6}Li + ^{12}C optical model parameters to better fit the current data set, using the code SFRESCO. We found that adjusting only the imaginary diffuseness a_I of the original
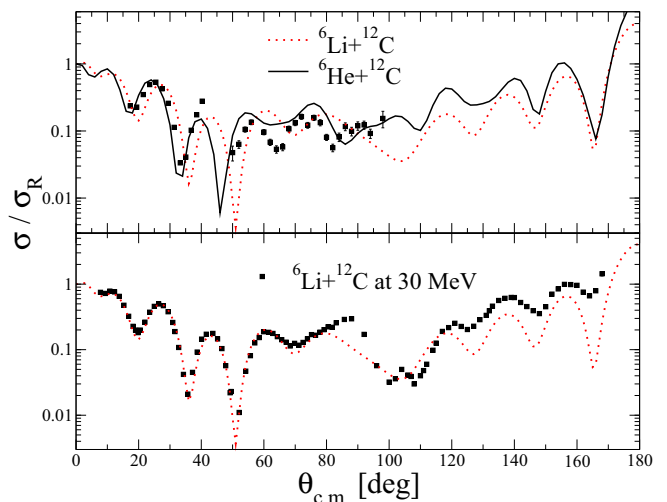

FIG. 5. (Color online) The elastic scattering angular distribution. The top figure shows ^{6}He + ^{12}C elastic scattering at $E_{\mathrm{lab}} = 30$ MeV. The dotted red line is the theoretical cross section calculated using the optical model parameters for the ^{6}Li + ^{12}C at 30 MeV [39], while the solid line is the theoretical cross section calculated using the optical model parameters of ^{6}He + ^{12}C obtained from the fit to the current data set. The bottom figure shows the ^{6}Li + ^{12}C elastic scattering at $E_{\mathrm{lab}} = 30$ MeV with the dotted red line being the optical model parameters for the ^{6}Li + ^{12}C at 30 MeV [39].

TABLE I. Optical model parameters used in this work. Potential depths (V, W, V_{SO}) are in units of MeV, radii (r_C, r_R, r_I, r_{SO}) and diffuseness (a_R, a_I, a_{SO}) are in units of fm. All referenced radius units are $R_x = r_x A_t^{1/3}$, where A_t corresponds to the number of nucleons in the target (t).

	r_C	V	r_R	a_R	W	r_I	a_I	V_{SO}	r_{SO}	a_{SO}
^{6}He+^{12}C/^{5}He+^{13}C	2.3	240.3	1.18	0.74	10.0	2.10	1.18			
^{6}Li+^{12}C [39]		2.3	240.3	1.18	0.74	10.0	2.10	0.78		
α+^{12,14}C [40]		1.2	40.69	2.12	0.1	2.21	2.98	0.22		
n+^{5}He [41]		1.2	4.3	1.25	0.65				6	1.25	0.65

^{6}Li potential and introducing the correct Coulomb charge, a good description of the ^{6}He was obtained [see the solid line in Fig. 5 (top)]. Similar adjustments were performed by Sakaguchi *et al.* [43] to the ^{6}Li + p optical potential to describe the ^{6}He + p scattering. We note that, while our ^{6}He scattering is measured out to $\theta_{c.m.} < 100°$, the elastic scattering data for ^{6}Li + ^{12}C [44] [see Fig. 5 (bottom)] goes out to much larger angles ($5° < \theta_{c.m.} < 170°$), and these large angles appear to be critical to better constrain the optical potential. The optical model parameters used for the elastic scattering are shown in Table I.

General features of the scattering can be observed from the ^{6}Li + ^{12}C optical model [39] at 30 MeV [see Fig. 5 (bottom)]. However, the current data have a notable shift in minima compared to the ^{6}Li + ^{12}C optical potential. This same effect was observed in the elastic scattering at 18 MeV of ^{6}He + ^{12}C by Milin *et al.* [22]. Using the adjusted elastic potential parameters, an analysis was performed for the inelastic scattering to the 2^+ 4.4 MeV state of ^{12}C.

B. Inelastic scattering (2^+ 4.4 MeV state)

Inelastic scattering of the 2^+ 4.4 MeV state of ^{12}C was observed and is shown in Fig. 4. The data were extracted and analyzed independently of the transfer model. A quadrupole deformation of ^{12}C was assumed with a deformation length of $\delta_l = -1.34$ fm taken from the analysis of inelastic scattering of ^{12}C + ^{6}Li at 30 MeV [45]. The coupling strength is calculated within the simple rotor model. A coupled-channel calculation with coupling between the ground state and first excited state of ^{12}C was assumed. The inelastic angular distribution is shown in Fig. 6. The adjustment of the imaginary diffuseness a_I as described in Sec. IV A, has the effect of decreasing the magnitude of the angular distribution at higher angles, improving the agreement with the data. In this work we do not couple the inelastic scattering contributions into the two-neutron transfer.

C. ^{12}C(^{6}He,^{4}He)^{14}C (2^+, 8.32 MeV)

The two-neutron transfer was extracted beyond background for all areas of detection except the UCD. Interference with the (p,t) reaction kinematics was observed and this led to the exclusion of events between $10.7° < \theta_{lab} < 19°$. The DCD/DBx relied on particle identification of the alpha particles from the ΔE-E spectrum. Coincident events were
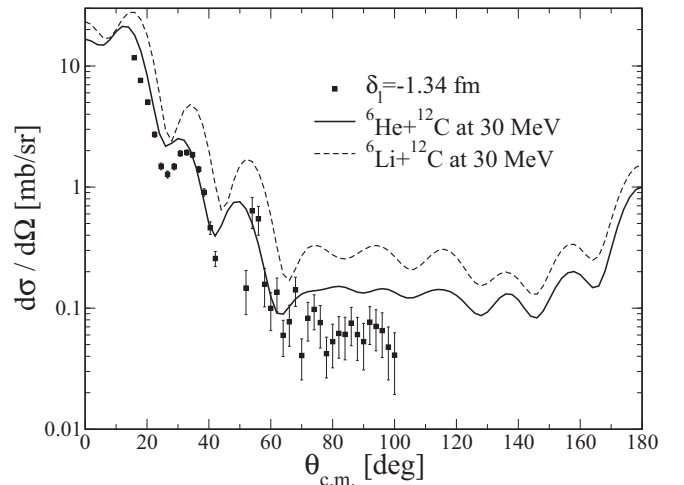

FIG. 6. The inelastic scattering to the 2^+ 4.4 MeV state. An independent model of the transfer was performed with the elastic scattering optical potential described above (see text for details).

selected for the DBx in a similar manner to that discussed in Sec. IV A. Background in the DBx and UBx was present due to a worsening of the angular resolution which was accounted for and subtracted from the spectrum.

The excitation spectrum of the two-neutron transfer for the DCD is shown in Fig. 7. The ground state (not shown) is only weakly populated due to Q value mismatching, and thus is not further discussed. Angular distributions for the closely spaced ^{14}C bound states could not be extracted due to the lack of ^{4}He-γ coincidences. Hence only the angular distribution for the 2_2^+ 8.32 MeV state of ^{14}C could be extracted.

The optical potentials used in the transfer calculations are shown in Table I. The elastic scattering parameters from
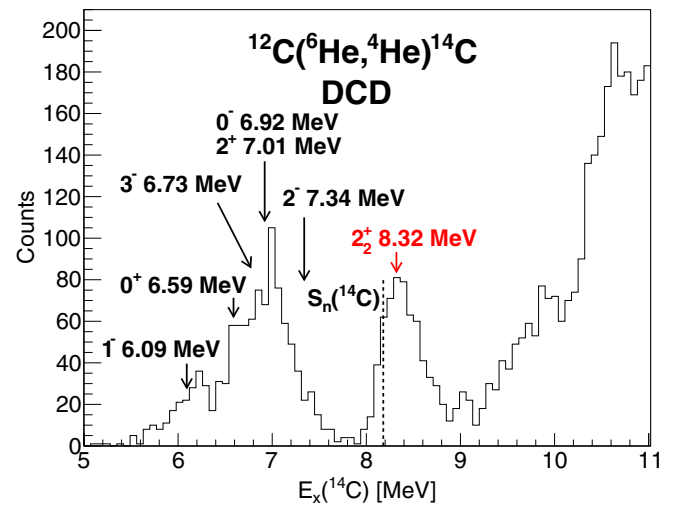

FIG. 7. (Color online) The energy excitation spectrum for the two-neutron transfer in the DCD. Separation of the 2_2^+ 8.32 MeV of ^{14}C is clearly observed. A high density of bound states from 6 to 7.3 MeV is observed, but cannot be separated without ^{4}He-γ coincidences. The 8.32 MeV state is located 200 keV above the neutron separation energy ($S_n = 8.1$ MeV).
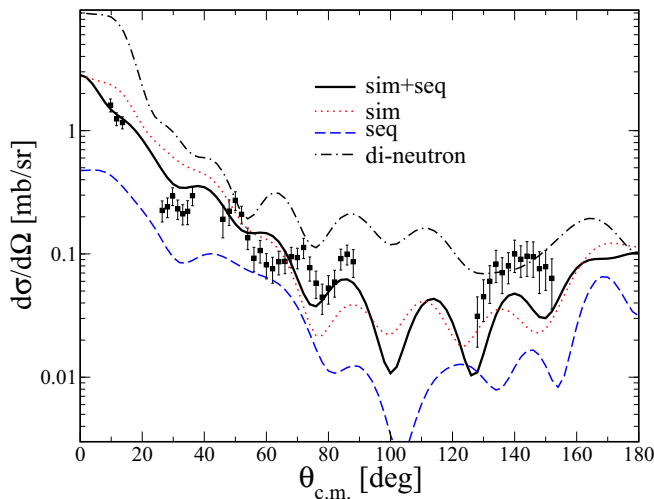
FIG. 8. (Color online) Comparison of the angular distribution of the ^{12}C(^{6}He,^{4}He)^{14}C 2^+ $E_x = 8.32$ MeV state at $E_{lab} = 30$ MeV with the current model. The dotted red line is the simultaneous two-neutron transfer accounting for the three-body nature of ^{6}He, the dashed blue line is the sequential two-step transfer accounting for the structure of ^{13}C, and ^{14}C and the solid black line is the coherent sum of the simultaneous and sequential transfer. For comparison, the dot-dashed black line is the simple dineutron model. See text for details.

FIG. 9. (Color online) Comparison of the angular distribution of the ^{12}C(^{6}He,^{4}He)^{14}C 2^+ $E_x = 8.32$ MeV state at $E_{lab} = 18$ MeV with the current model. Refer to Fig. 8 for the description of the lines and the text for details.

Sec. IV A were used as the entrance channel and the ^{5}He $+ \, ^{13}$C interaction potentials. For the exit channel and the core-core potential, $\alpha + \, ^{12}$C data at 28.2 MeV [40] was fit using SFRESCO. For the $n + \, ^{12}$C binding potential, we took a standard radius and diffuseness, and adjusted the depth to reproduce the correct binding energy. A Gaussian potential was used for the $\alpha + n$ binding potential [15] and finally the ^{5}He $+ \, n$ binding potential was taken from Keeley et al. [41].

The 2^+_2 8.32 MeV transfer cross section is shown in Fig. 8. Note that only statistical errors are included for the data. The reaction calculations agree fairly well with the data, considering no normalization factor is applied to the transfer (no unhappiness factor). The solid black line corresponds to the coherent sum of the sequential and simultaneous transfer, the dotted red line is the simultaneous transfer alone, and the dashed blue line is the result of including the sequential transfer contributions only.

We performed various sensitivity tests to assess the robustness of our results. We found that taking the intermediate levels as degenerate introduces a reduction of the cross section by no more than $\approx 5\%$. However, the transfer cross section is by far most sensitive to the choice of the optical potentials. Taking a different set of parameters for an optical potential describing the ^{6}He $+ \, ^{12}$C elastic scattering, resulted in significant effects on the magnitude (up to 50%) as well as on the shape of the angular distribution. The effects of similar magnitude were seen for changes in the exit optical potential and in the core-core interaction. Less significant were the effects of the geometry used for the binding potentials of ^{12}C $+ n/^{13}$C $+ n$. In all cases the simultaneous two-neutron transfer remained the dominant component. However, the interplay between the
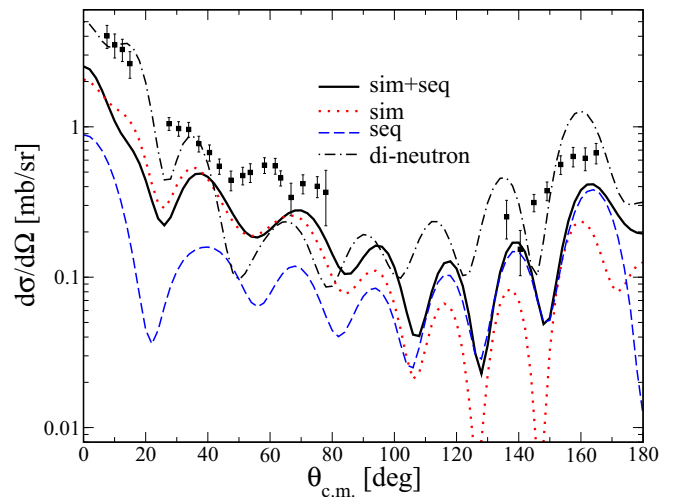
simultaneous and sequential transfer provides a better overall agreement with the data.

For completeness, we examine the same reaction at 18 MeV [22]. The entrance channel (^{6}He $+ \, ^{12}$C), exit channel (^{4}He $+ \, ^{14}$C), and sequential channel (^{5}He $+ \, ^{13}$C) were adjusted to those used by Milin et al. [46]. All structure information introduced in this calculation was kept the same as that used for the analysis of the 30 MeV reaction, for a meaningful comparison. As can be seen, the angular distributions presented in Fig. 9 show a systematic underestimation of the experimental cross section.

A comparison with the pure dineutron model was made for both the 30-MeV data and the 18-MeV data. We use the same binding potentials in Milin et al. [22], for ^{12}C $+ 2n$ and ^{4}He $+ 2n$, keeping the optical potentials unchanged. In ^{6}He, we assumed the two neutrons were transferred from a relative $2S$ state. The results obtained with the dineutron model are shown in Figs. 8 and 9 by the dot-dashed line. Applying a renormalization of ≈ 0.3 to the 30-MeV dineutron cross section (not shown in Fig. 8) produces a distribution that resembles the respective data. The dineutron model appears to better describe the 18-MeV data, particularly at forward and backward angles without any normalization. Also, a coupled-channel analysis of the 18-MeV data [47] including elastic, inelastic, and transfer channels, again based on the simple dineutron model, produces cross sections in agreement with the data. However, the agreement of the dineutron model with the 18-MeV data is deceptive. The fact that our simultaneous transfer predictions (the dotted lines in Figs. 8 and 9) are far from the dineutron predictions (dot-dashed lines) stress the need for the inclusion of the correct three-body description of the projectile since it introduces important dynamics in the process.

While it is reassuring that the best reaction model is able to describe our transfer data at 30 MeV, the factor of 2 mismatch between our best reaction model and the data at 18 MeV, shown in Fig. 9, calls for further investigation. Ideally, as a

first step, one should perform a more thorough study of the optical potential parameter sensitivities at this energy. Next, one should study the effect of inelastic and continuum channels in the reaction mechanism. Such work is, however, well beyond the scope of the present paper.

V. CONCLUSION

In summary, the elastic scattering of ^{6}He on ^{12}C at 30 MeV was measured and an angular distribution extracted. Inelastic scattering data were also extracted and analyzed including the quadrupole deformation of ^{12}C. Qualitative agreement to the data was found, when accounting for full coupling of the ground state and first excited state of ^{12}C. Data for the two-neutron transfer angular distribution to the 2_2^+ 8.32 MeV state in ^{14}C were observed and analyzed, including the simultaneous and the sequential contributions. A realistic three-body structure for ^{6}He was taken into account and state-of-the-art shell-model predictions were used for the structure of the carbon isotopes.

Overall, the reaction model describes the new data without invoking a normalization constant. It was observed that the simultaneous transfer is the dominant reaction mechanism, yet the strong interplay between the intermediate states of ^{13}C have nonnegligible contributions to the final results. This implies that adding the two-step process is required to better account for the overall reaction mechanism. Discrepancies observed when adopting the current model to data at 18 MeV show that further theoretical work is required for a general and reliable approach to (^{6}He,^{4}He) reactions. Even with the simultaneous experimental measurement

of the elastic scattering, we find that the largest source of uncertainties in the calculation lies in the determination of the optical model potentials. Our sensitivity studies suggest that measurements of the elastic scattering all the way to 170° could reduce these uncertainties. This, however, presents some serious experimental challenges.

Concerning the reaction theory for the two-neutron transfer, this calls for further developments. Future work should include the study of the effects of the continuum (e.g., the 2^+ ^{6}He resonance, the ^{5}He states, etc.) in the reaction dynamics. The strong sensitivity to the choice of optical potential parameters may be greatly reduced, if these are derived microscopically. Finally, comparisons to multiple final bound states of ^{14}C, such as the first 0^+ and 2^+ states, would allow a more thorough understanding of the spin dependencies of one-step and two-step processes.

[1] I. J. Thompson, in *Fifty Years of Nuclear BCS: Pairing in Finite Systems*, edited by R. A. Broglia and V. Zelevinsky (World Scientific, Singapore, 2013), Chap. 34.

[2] I. Tanihata *et al.*, Prog. Part. Nucl. Phys. **68**, 215 (2013).

[3] P. Decowski *et al.*, Nucl. Phys. A **302**, 186 (1978).

[4] J. Bjerregaard *et al.*, Nucl. Phys. A **110**, 1 (1968).

[5] K. Wimmer *et al.*, Phys. Rev. Lett. **105**, 252501 (2010).

[6] G. Potel, F. Barranco, F. Marini, A. Idini, E. Vigezzi, and R. A. Broglia, Phys. Rev. Lett. **107**, 092501 (2011).

[7] U. Gatz *et al.*, Phys. Rep. **16**, 115 (1975).

[8] M. Igarashi *et al.*, Phys. Rep. **199**, 1 (1991).

[9] M. C. Mermaz *et al.*, Phys. Rev. C **20**, 2130 (1979).

[10] P. Kunz *et al.*, Phys. Lett. B **112**, 5 (1982).

[11] A. Chatterjee *et al.*, Phys. Rev. Lett. **101**, 032701 (2008).

[12] K. Varga, Y. Suzuki, and Y. Ohbayasi, Phys. Rev. C **50**, 189 (1994).

[13] I. Brida and F. Nunes, Nucl. Phys. A **847**, 1 (2010).

[14] L. Fortunato *et al.*, Euro. Phys. J A **14**, 37 (2002).

[15] M. Zhukov *et al.*, Phys. Rep. **231**, 151 (1993).

[16] I. Tanihata *et al.*, Phys. Rev. Lett. **55**, 2676 (1985).

[17] R. Wolski *et al.*, Joint Institute for Nuclear Research Report No. E15-98-284, 1998.

[18] L. Giot *et al.*, Phys. Rev. C **71**, 064311 (2005).

[19] R. Raabe *et al.*, Phys. Rev. C **67**, 044602 (2003).

[20] G. Ter-Akopian *et al.*, Phys. Lett. B **426**, 251 (1998).

[21] A. N. Ostrowski *et al.*, J. Phys. G **24**, 1553 (1998).

[22] M. Milin *et al.*, Nucl. Phys. A **730**, 285 (2004).

[23] I. Krouglov and W. Oertzen, Eur. Phys. J. A **8**, 501 (2000).

[24] C. A. Diget *et al.*, J. Instrum. **6**, P02005 (2011).

[25] G. Hackman and C. Svensson, Hyperfine Interactions **225**, 241 (2013).

[26] Y. T. Oganessian, V. I. Zagrebaev, and J. S. Vaagen, Phys. Rev. C **60**, 044605 (1999).

[27] I. J. Thompson and F. M. Nunes, *Nuclear Reactions for Astrophysics* (Cambridge Unviersity Press, Cambridge, England, 2009).

[28] N. K. Timofeyuk, Phys. Rev. C **63**, 054609 (2001).

[29] I. Brida and F. M. Nunes, Int. J. Mod. Phys. E **17**, 2374 (2008).

[30] J. Al-Khalili *et al.*, Phys. Lett. B **378**, 45 (1996).

[31] V. Lapoux *et al.*, Phys. Rev. C **66**, 034608 (2002).

[32] E. K. Warburton and W. T. Pinkston, Phys. Rev. **118**, 733 (1960).

[33] S. Lie, Nucl. Phys. A **181**, 517 (1972).

[34] S. Mordechai *et al.*, Nucl. Phys. A **301**, 463 (1978).

[35] B. A. Brown, W. D. M. Rae, E. McDonald, and M. Horoi, NUSHELLX@MSU, http://www.nscl.msu.edu/~brown/resources/resources.html; W. D. M. Rae, NUSHELLX, http://www.garsington.eclipse.co.uk/

[36] Y. Utsuno and S. Chiba, Phys. Rev. C **83**, 021301 (2011).

[37] I. J. Thompson, Comput. Phys. Rep. **7**, 167 (1988).

[38] http://www.fresco.org.uk/programs/efaddy/

[39] D. E. Trcka, A. D. Frawley, K. W. Kemper, D. Robson, J. D. Fox, and E. G. Myers, Phys. Rev. C **41**, 2134 (1990).

[40] T. Mikumo, J. Phys. Soc. Jpn. **16**, 1066 (1961).

[41] N. Keeley and N. Alamanos, Phys. Rev. C **77**, 054602 (2008).

[42] S. Agostinelli *et al.*, Nucl. Instrum. Methods A **506**, 250 (2003).

[43] S. Sakaguchi *et al.*, Phys. Rev. C **84**, 024604 (2011).

[44] M. F. Vineyard, J. Cook, K. W. Kemper, and M. N. Stephens, Phys. Rev. C **30**, 916 (1984).

[45] P. L. Kerr, K. W. Kemper, P. V. Green, K. Mohajeri, E. G. Myers, B. G. Schmidt, and V. Hnizdo, Phys. Rev. C **54**, 1267 (1996).

[46] D. R. Ober and O. E. Johnson, Phys. Rev. **170**, 924 (1968).

[47] I. Boztosun, M. Karakoc, and Y. Kucuk, Phys. Rev. C **77**, 064608 (2008).